ResearchGate

See discussions, stats, and author profiles for this publication at: https://www.researchgate.net/publication/227587996

Exact Computation and Asymptotic Approximations of 6j Symbols: Illustration of Their Semiclassical Limits

ARTICLE *in* INTERNATIONAL JOURNAL OF QUANTUM CHEMISTRY · MARCH 2010

Impact Factor: 1.43 · DOI: 10.1002/qua.22117

CITATIONS
14

READS
19

6 AUTHORS, INCLUDING:

Mirco Ragni

22 PUBLICATIONS **233** CITATIONS

SEE PROFILE

Ana Carla Bitencourt

Universidade Estadual de Feira de Santana

23 PUBLICATIONS **237** CITATIONS

SEE PROFILE

Vincenzo Aquilanti

Università degli Studi di Perugia

315 PUBLICATIONS **6,414** CITATIONS

SEE PROFILE

Available from: Mirco Ragni
Retrieved on: 25 January 2016

Exact Computation and Asymptotic Approximations of 6*j* Symbols: Illustration of Their Semiclassical Limits

MIRCO RAGNI,[1] ANA CARLA PEIXOTO BITENCOURT,[1,*] CRISTIANE DA S. FERREIRA,[1] VINCENZO AQUILANTI,[1] ROGER W. ANDERSON,[2] ROBERT G. LITTLEJOHN[3]

[1]*Dipartimento di Chimica, Università di Perugia, 06123 Perugia, Italy*

[2]*Department of Chemistry, University of California, Santa Cruz, CA 95064*

[3]*Department of Physics, University of California, Berkeley, CA 94720*

Received 31 December 2008; accepted 13 January 2009
Published online 23 June 2009 in Wiley InterScience (www.interscience.wiley.com).
DOI 10.1002/qua.22117

ABSTRACT: This article describes a direct method for the exact computation of 3*nj* symbols from the defining series, and continues discussing properties and asymptotic formulas focusing on the most important case, the 6*j* symbols or Racah coefficients. Relationships with families of hypergeometric orthogonal polynomials are presented and the asymptotic behavior is studied to account for some of the most relevant features, both from the viewpoints of the basic geometrical significance and as a source of accurate approximation formulas, such as those due to Ponzano and Regge and Schulten and Gordon. Numerical aspects are specifically investigated in detail, regarding the relationship between functions of discrete and of continuous variables, exhibiting the transition in the limit of large angular momenta toward both Wigner's reduced rotation matrices (or Jacobi polynomials) and harmonic oscillators (or Hermite polynomials). © 2009 Wiley Periodicals, Inc. Int J Quantum Chem 110: 731–742, 2010

Key words: Racah–Wigner coefficients; fast computation of 6*j*-symbols; test of approximations; Ponzano–Regge; Schulten–Gordon

Correspondence to: M. Ragni; e-mail: mirco.ragni@gmail.com
Present address: Centro de formação de professores, Universidade Federal do Recôncavo de Bahia, Amargosa, Brasil.
Contract grant sponsors: Italian MUR, ASI.

© 2009 Wiley Periodicals, Inc.

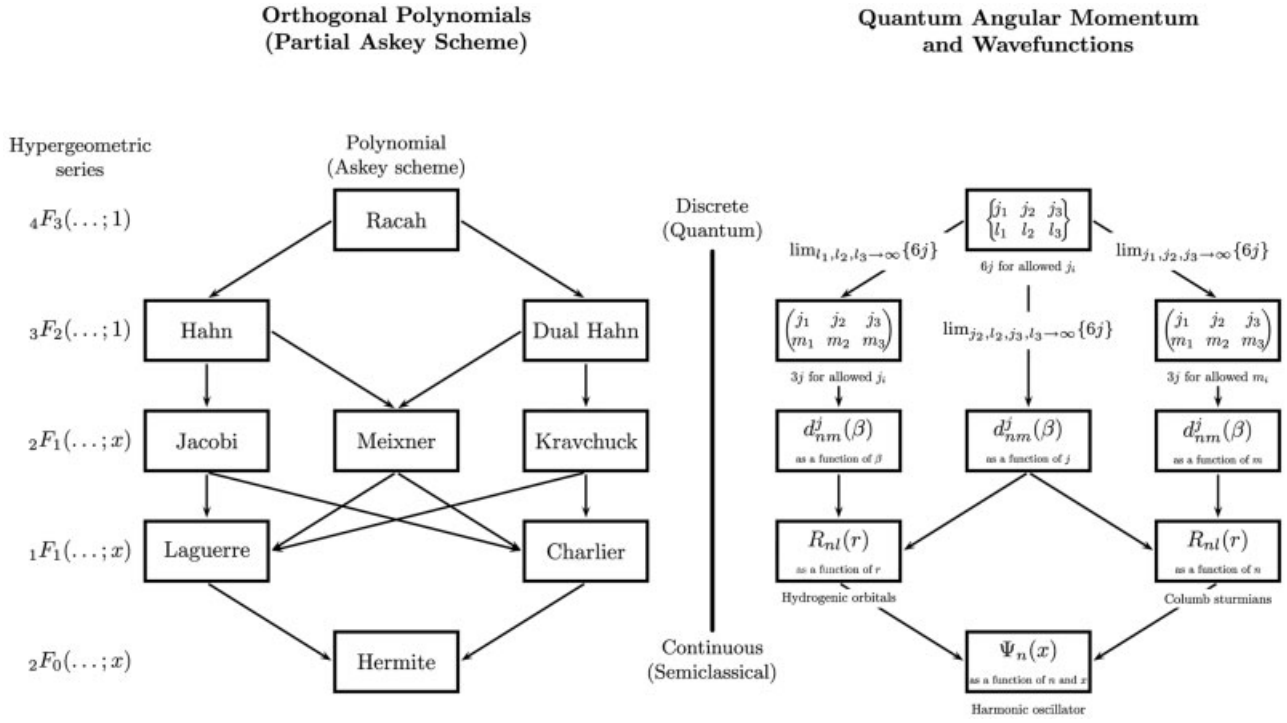

FIGURE 1. Comparative classifications of orthogonal hypergeometric polynomials (left scheme) and of ingredients of quantum theory of angular momentum and wave-functions (right scheme). The downward connections are limiting relationships which physically correspond to semiclassical limits, while going upwards one has a ladder for representing complete sets of orthogonal functions on discrete grids. See also [34] and [3].

1. Introduction

This article contains a presentation of properties, useful formulas, and exemplary illustrations for a basic mathematical tool, the 6*j*-symbol, also known in quantum mechanical angular momentum theory as Racah coefficient and the building block of 3*nj*-symbols and spin networks. See [1, 2] for an updated account of spin networks, as well as of their applications in quantum physics and chemistry, and also more recently in quantum gravity and quantum computing. Both exact computation codes and important asymptotic approximations are given and tested, their use being emphasized for semiclassical problems and for discretization algorithms.

Basic connections among the 6*j* symbols of angular momentum theory with both the theory of superposition coefficients of hyperspherical harmonics and the theory of discrete orthogonal polynomials have been reviewed in [3, 4]. In Ref. [3], we also sketched a connection between the Askey scheme of orthogonal polynomials and the tools of angular momentum theory (6*j*, 3*j*, rotation *d*-matrices,. . .), going down the scheme corresponding in quantum mechanics to the semiclassical limit, while going up provides discretization algorithms for quantum mechanical calculations (for example, our hyperquantization algorithm). Reference is made to Figure 1. This work starts by updating the former one [3] by accounting on recent progress and then presents illustrations of exact and asymptotic formulas of relevance for applications.

Explicit expressions for the 6*j* coefficients can be written according to the series expressions of the Racah type, or as generalized hypergeometric series, or in connection with the so-called Racah polynomials. Orthogonal polynomials of a discrete variable are important tools of numerical analysis for the representation of functions on grids. As matrix elements of the overlap between spherical and hyperspherical harmonics [3, 6], they occur in quantum chemistry as momentum space (or Sturmian) orbitals [7, 8]. We exploited both their connection with the coupling and recoupling coefficients of angular momentum theory [9] and their asymptotic

relationships (semiclassical limit) [10] to develop a discretization procedure, the hyperquantization algorithm, applied to the study of anisotropic interactions and of reactive scattering as a quantum mechanical n-body problem. Use for fitting of potential energy surfaces has been also proposed and further applications have been made to stereodirected dynamics via an exact representation for scattering matrix as well as to the characterization of atomic and molecular polarizations [11].

The scheme of this article is as follows. The next section provides the general setting for the computation of generalized hypergeometric functions by direct summation of the defining series and their specific application for the efficient calculation of functions occurring in angular momentum theory, 6j-symbols (or Racah coefficients), the 3j symbols (or Clebsch–Gordan coefficients), and Wigner's d matrices by the direct evaluation of the corresponding hypergeometric or generalized hypergeometric series. The following section outlines the connections between angular momentum algebra and special functions, with particular reference to orthogonal polynomials of the hypergeometric family. This allows us to elaborate further on the classification scheme of Figure 1 which exhibits asymptotic relationships, which play a role in the study of the semiclassical limit. The powerful geometrical view essentially due to Ponzano and Regge [12] is illustrated (Section 3) with particular reference to the approach of Schulten and Gordon [13], based on the asymptotic mapping of an exact three-term recursive relationship into a Schrödinger-like differential equation. The relationship is also presented with harmonic oscillator wavefunctions in particular cases. Conclusions follow in Section 5.

2. Computation of Mathematical Functions and Angular Momentum 3*nj*-Symbols

We calculate the 3nj-symbols and Wigner d functions by directly summing the defining series using multiprecision arithmetic (MPFUN90 [14]). The multiple precision arithmetic allows convenient calculation of hypergeometric functions, ${}_pF_q$, of small and large argument by their series definition,

$$ {}_pF_q(a_1,a_2,\ldots,a_p;b_1,b_2,\ldots,b_q;z) = \sum_{k=0}^{\infty} \frac{(a_1)_k(a_2)_k\ldots(a_p)_k z^k}{(b_1)_k(b_2)_k\ldots(b_q)_k k!}, \quad (1) $$

$$ (a_k) = a(a+1)\ldots(a+k+1) = \frac{\Gamma(a+k)}{\Gamma(a)}, \quad (2) $$

and without the necessity of using recurrence relations, integral and rational representations, or asymptotic approximations. The formulas for the functions used in this work are found in Varshalovich [15]: d functions with ${}_2F_1$ [p. 78, Eq. (16)]

$$ d^J_{M,M'}(\beta) = \frac{\xi_{M,M'}}{\mu!}\left[\frac{(s+\mu+\nu)!(s+\mu)!}{s!(s+\nu)!}\right]^{1/2}\left(\sin\frac{\beta}{2}\right)^{\mu}\left(\cos\frac{\beta}{2}\right)^{\nu} {}_2F_1\left(-s, s+\mu+nu+1; \mu+1; \sin^2\frac{\beta}{2}\right), \quad (3) $$

$\mu = |M - M'|, \nu = |M + M'|, s = J - 1/2(\mu + \nu)$, $\xi_{M,M'} = 1$ for $M' > M$, $\xi_{M,M'} = (-1)^{M'-M}$ for $M' < M$. Clebsch–Gordan coefficients and 3j-symbols with ${}_3F_2$ [p. 236, Eq. (11); p. 241, Eq. (25)]

$$ \begin{pmatrix} j_1 & j_2 & j_3 \\ m_1 & m_2 & m_3 \end{pmatrix} = (-1)^{j_3+m_3+2j_1}\frac{1}{\sqrt{2j_3+1}}\langle j_1 j_2 - m_1 - m_2 | j_3 m_3\rangle, $$

$$ \Delta(a,b,c) = \left[\frac{(a+b-c)!(a-b+c)!(-a+b+c)!}{(a+b+c+1)!}\right]^{1/2} $$

$$ \langle j_1 j_2 m_1 m_2 | jm\rangle = \frac{\delta_{m,m_1+m_2}(-1)^{j_2+m_2}\Delta(j_1,j_2,j)(2j)!(j+j_2+m_1)!}{(j_1-j_2+j)!(-j_1+j_2+j)!} \left[\frac{(j_1-m_1)!(2j+1)!}{(j_1+m_1)!(j_2+m_2)!(j_2-m_2)!(j+m)!(j-m)!}\right]^{1/2} {}_3F_2\left[\begin{matrix} j_1-j_2-j, -j_1-j_2-j-1, -j-m \\ -2j, -j_2-j-m_1 \end{matrix}\middle| 1\right]. \quad (4) $$

6j-symbols with ${}_4F_3$ [p. 295, Eq. (10)]:

$$ \begin{Bmatrix} a & b & c \\ d & e & f \end{Bmatrix} = \frac{\Delta(a,b,c)\Delta(b,d,f)}{\Delta(a,e,f)\Delta(c,d,e)} $$

$$\frac{\begin{array}{c}(a-b+d+e)!(-b+c+e+f)!\\(a+c+d+f+1)!\end{array}}{\begin{array}{l}(a-b+c)!(-b+d+f)!(a+e+f+1)!\\(b+d+e+1)!(-a+c-d+f)!\\(-b+c-e+f)!\end{array}}$$

$${}_4F_3[-a+b-c, b-d-f, -a-e-f-1, -c-d-e-1-a+b-d-e, b-c-e-f, -a-c-d-f-1|1]. \quad (5)$$

We note that some of the other equations expressing Clebsch–Gordan coefficients ([15] pp. 240–241) and 6*j*-symbols (p. 295) with hypergeometric functions do not always give correct results. However, the equations cited above appear to work properly with our extensive testing. The 9*j*-symbols are evaluated with Eq. (1) and general 3*nj*-symbols can be calculated by their definition as summations over 6*j*-symbols. For 9*j*, see also recent paper [16] and reference therein.

The basic problem in these calculations is that sums are generally used for such calculations, and some of the terms in the sum may become very large ($\sim 10^{100}$ or larger). However, the sum must be a number in the range $[-1,1]$. With normal precision (8 to 32 decimal places), it is clear that direct summation will not generally produce accurate results. However, multiple precision arithmetic packages [14] that allow calculations with thousands (or millions!) of digits sum the hypergeometric series easily for j_i of magnitude much larger than one thousand.

For many years Clebsch–Gordan coefficients, 3*j*-symbols, and 6*j*-symbols have been calculated for small j with algebraic sums (Varshalovich [15] [pp. 238, 294], Zare [17] [pp. 49, 146, 328–333]), binomial coefficients (Varshalovich [15] [p. 240], Labarthe [18], Roothaan and Lai [19], Hinze, unpublished), and formulas for special cases (Varshalovich [15] [pp. 248–252, 299–303], Zare [17] [pp. 57–61, 169–171]). Recurrence relations are often used for large j (Varshalovich [15] [pp. 252–257, pp. 303–304], Schulten and Gordon [20, 21]). See also [3] and next section. However there are six arguments in the definition of the Clebsch–Gordan coefficient $\langle j_1,j_2,m_1,m_2|j,m\rangle$, and hence there are many different recurrence formulas.

Some other researchers in recent years have written specialized multiprecision arithmetic programs [22] to calculate Clebsch–Gordan coefficients, 6*j*-symbols, and 9*j*-symbols. But a recent published calculation [23] of 12*j*-symbols is mostly incorrect. A Java calculator [24] using BigInteger has been written for evaluation of 3*j*-, 6*j*-, and 9*j*-symbols. There are numerous applications for symbolic software programs to evaluate recoupling coefficients: for example, Scheme [25], Maple [26–29], Mathematica [30], and Macsyma [31] (Maxima). However we chose the MPFUN90 [14] package, because it is so easily integrated and optimized in Fortran 90/95 programs. The ARPREC [14] package provides equivalent results.

The asymptotic behavior for 3*nj*-symbols of large argument has been occasionally studied [32, 33] (Ponzano and Regge [12], Schulten and Gordon [13], Varshalovich [pp. 264–267, 306–310]), and very useful and accurate formulas are available. For 9*j* see [16]

3. Semiclassical Limits and Schulten–Gordon Approach

The Askey scheme for orthogonal polynomials of hyperspherical family and its counterpart for the tools of angular momentum theory are shown in Figure 1. Arrows pointing out downwards are asymptotic connections. Most of the limiting formulas appearing in the diagrams are available in the literature, although often in forms which are not of immediate use. Also, they can be derived in many ways. In view of the following steps, we consider a powerful source of both transparent results and of physical insight in those derivations which are based on three-terms recursion relationships. A basic role is played by the relationship which relates three 6*j* symbols with an argument differing by one $\langle j_1 - 1, j_1, j_1 + 1\rangle$, notation follows [3]:

$$j_{23}E(j_{23}+1)\begin{Bmatrix} j_1 & j_2 & j_{12} \\ j_3 & j & j_{23}+1 \end{Bmatrix} + F(j_{23})\begin{Bmatrix} j_1 & j_2 & j_{12} \\ j_3 & j & j_{23} \end{Bmatrix} + (j_{23}+1)E(j_{23})\begin{Bmatrix} j_1 & j_2 & j_{12} \\ j_3 & j & j_{23}-1 \end{Bmatrix} = 0, \quad (6)$$

where

$$E(j_{23}) = \{[j_{23}^2 - (j-j_1)^2][(j+j_1+1)^2 - j_{23}^2][j_{23}^2 - (j_3-j_2)^2][(j_2+j_3+1)^2 - j_{23}^2]\}^{1/2}$$

$$F(j_{23}) = (2j_{23}+1)\{j_{23}(j_{23}+1)[-j_{23}(j_{23}+1) + j_2(j_2+1) + j_3(j_3+1)] + j_1(j_1+1)[j_{23}(j_{23}+1) - j_2(j_2+1) + j_3(j_3+1)]$$

$$+ j(j+1)[j_{23}(j_{23}+1) + j_2(j_2+1) - j_3(j_3+1)] - 2j_{23}(j_{23}+1)j_{12}(j_{12}+1)\}. \quad (7)$$

In this formula, one can introduce a quantity R such that either and $m_1 = j_{23} - j$, $m_2 = j_3 - j_{23}$, $m_3 = j - j_3$. We have

$$j_3 = R + \frac{m_2 - m_3}{2},\ j = R + \frac{m_2 + m_3}{2},\ \text{and}\ j_{23} = R - \frac{m_2 + m_3}{2}. \quad (8)$$

So that when R goes to infinity, we obtain a three-terms recurrence relationship for the $3j$ symbols as a function of j_1 (i.e., essentially the Hahn polynomials). Analogously, but taking

$$j_1 = R + \frac{m_2 - m_3}{2},\ j_2 = R + \frac{m_2 + m_3}{2},\ \text{and}\ l_3 = R - \frac{m_2 + m_3}{2}. \quad (9)$$

when R goes to infinity, we obtain another three-term recurrence relationship for the $3j$ symbols as function of m_2 (i.e., essentially the dual Hahn polynomials). See [34] for details of the connection of $3j$ symbols with Hahn polynomials, and for examples illustrating asymptotic relationships to d-matrices.

Further relationships tie $6j$ and $3j$ symbols to d matrices, many being equivalent to equations in orthogonal polynomial theory (See Ref. [4, 5]). They have served to understand the semiclassical limit, but also in the hyperquantization algorithm to represent a continuous function by a discrete one, which can be exploited for numerical applications, such as the solution of Schrödinger equation in quantum mechanical problems. Check and illustration of other formulas are interesting and useful. Below (Section 3.1.) we exemplify the passage from Racah polynomial to Jacobi or Meixner or Krawchuk polynomials, or equivalently from $6j$ symbol to the Wigner rotation matrix when all angular momenta can be large except one. These comparisons require accurate computations of e.g., $6j$, $3j$, and $d^j_{m,n}$ rotation matrices for large values of the entries. This has been for a long time a very demanding problem, circumvented by the use of three-term recurrence relationships, see for example Ref. [3, 9]. In the following, we exploit the direct program in multiple precision Fortran language, which has been described in Section 2 and permits us to make such comparisons between exact and asymptotic values.

3.1. WIGNER REDUCED ROTATION MATRIX ELEMENTS AS LIMITS OF 6*j* SYMBOLS

The $6j$ symbols tend asymptotically to Wigner $d^l_{nm}(\theta)$ functions when some angular momenta are large where θ assumes certain discrete values (Nikiforov, Eq. 5.3.16, p. 262).

$$\begin{Bmatrix} N+n & N & l \\ M+m & M & L \end{Bmatrix} \simeq \frac{(-1)^{N+M+m+L}}{\sqrt{(2N+n+1)(2M+m+1)}} d^l_{nm}(\theta_L) \quad (10)$$

and N and M are large. Inversely, we have a formula for the discrete analogue of rotation matrix elements:

$$d^l_{nm}(\theta_L) \simeq (-1)^{N+M+m+L}\sqrt{(2N+n+1)(2M+m+1)} \times \begin{Bmatrix} N+n & N & l \\ M+m & M & L \end{Bmatrix}. \quad (11)$$

In both formulas,

$$\cos(\theta_L) = \frac{(2L+1) - (2N+n+1) - (2M+m+1)}{2(2N+n+1)(2M+m+1)}. \quad (12)$$

These formulas, illustrated in Figure 2, are somewhat more accurate than similar ones, known since long time and corresponding to a direct passage from the top of Figure 1 down by two levels. See also [35] and references therein.

3.2. GEOMETRICAL INTERPRETATION

Equation (12) has an interesting geometrical interpretation, based on the vector model visualization of quantum angular momentum coupling by the triangle of vectors that we would draw in classical mechanics. Under such a perspective, $\pi - \theta_L$ can be perceived as the angle formed by the two sides of length $N + n/2 + 1/2$ and $M + m/2 + 1/2$ in a triangle (See Fig. 3) where $L + 1/2$ is the third side. Equivalently, θ_L can be seen as the angle which in that triangle is formed by the outer nor-

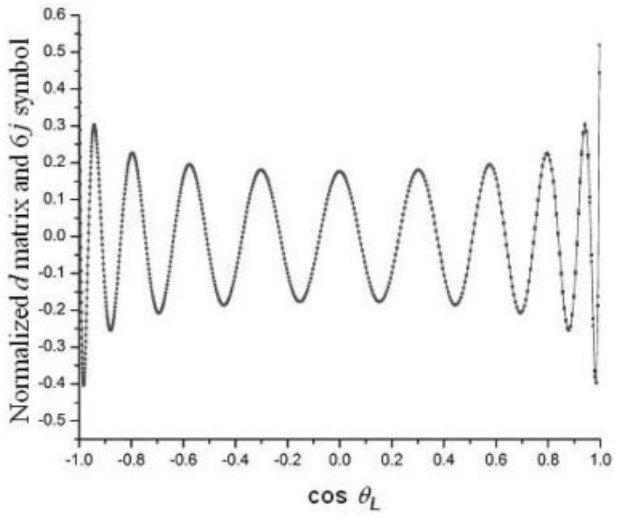

FIGURE 2. The picture is an illustration of Eqs. (10)–(12) for the case where in the $d^{l}_{nm}(\theta_L)$ $l = 20$, $n = 0$, and $m = 0$ (solid line). Dots are the normalized 6*j*-symbols of Eq. (11) with $N = M = 320$ and $L_{\max} = 640$.

mals to the two sides. In view of this and of a great deal of further evidence, in the following when we consider 6*j* properties as correlated to those of the tetrahedron of Figure 4, we use the substitution $J_x = j_x + 1/2$ which greatly improves all asymptotic formulas down to surprisingly low values of the entries.

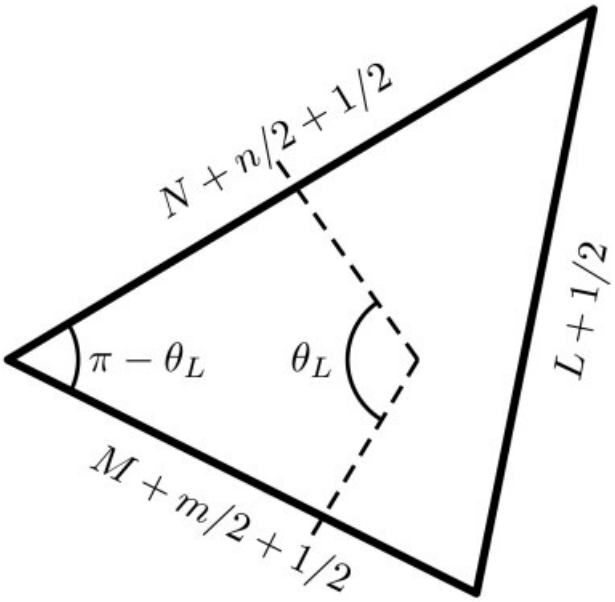

FIGURE 3. The triangle of Eqs. (10)–(12).

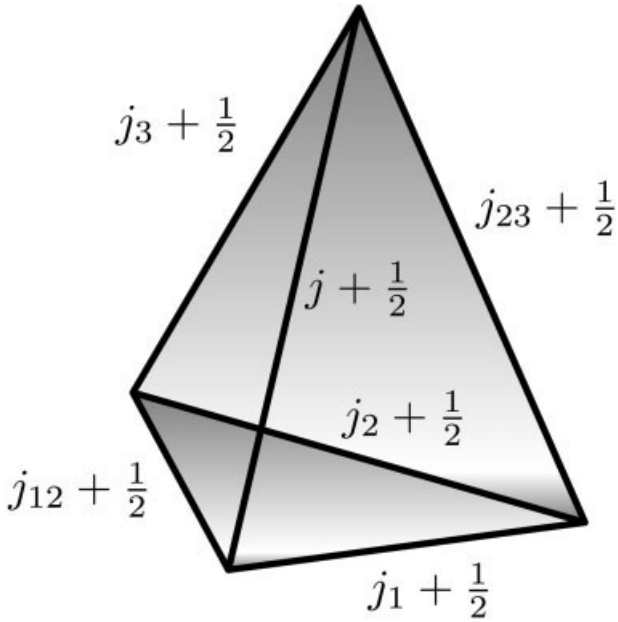

FIGURE 4. Ponzano-Regge tetrahedron built up with the six angular momenta appearing in the 6*j* symbol $\begin{Bmatrix} j_1 & j_2 & j_{12} \\ j_3 & j & j_{23} \end{Bmatrix}$.

The square of the area of each triangular face is given by the formula:

$$F^2(a,b,c) = \frac{1}{16}(a+b+c)(-a+b+c)(a-b+c) \times (a+b-c) = -\frac{1}{16}\begin{vmatrix} 0 & a & b & 1 \\ a & 0 & c & 1 \\ b & c & 0 & 1 \\ 1 & 1 & 1 & 0 \end{vmatrix}, \tag{13}$$

where *a*, *b*, *c* are the sides of the face. Similarly, the square of the volume of an irregular tetrahedron, such as the one in Figure 3, can be written as follows (the Cayley-Menger determinant):

$$V^2 = \frac{1}{288}\begin{vmatrix} 0 & J_3^2 & J^2 & J_{23}^2 & 1 \\ J_3^2 & 0 & J_{12}^2 & J_2^2 & 1 \\ J^2 & J_{12}^2 & 0 & J_1^2 & 1 \\ J_{23}^2 & J_2^2 & J_1^2 & 0 & 1 \\ 1 & 1 & 1 & 1 & 0 \end{vmatrix} \tag{14}$$

This can be reduced to a three by three determinant [36], at the expense of partial spoiling of the symmetry. When the values of J_1, J_2, J_{12}, J_3, and J are

fixed, the maximum value for the volume as a function of j_{23} is given at

$$j_{23}^{\max}+\frac{1}{2}=J_{23}^{V\max}=\left(\frac{\begin{array}{r}-J_2^2J_3^2+J_{12}^2J_3^2+J_1^2J_3^2+J_{12}^2J_2^2+J^2J_2^2\\ -J_{12}^4+J_1^2J_{12}^2+J^2J_{12}^2-J^2J_1^2\end{array}}{2J_{12}^2}\right)^{1/2}. \quad (15)$$

The corresponding volume is

$$V^{\max}(J_1,J_2,J_{12},J_3,J)=\frac{\sqrt{A_{1,2}A_{12,3}}}{24J_{12}}, \quad (16)$$

where

$$A_{1,2}=J_1^4+J_2^4+J_{12}^4-2(J_1^2J_{12}^2+J_1^2J_2^2+J_2^2J_{12}^2),$$
$$A_{12,3}=J^4+J_3^4+J_{12}^4-2(J^2J_{12}^2+J^2J_3^2+J_3^2J_{12}^2). \quad (17)$$

Therefore, the two values of J_{23} for which the volume is zero are:

$$j_{23}^{\pm}+\frac{1}{2}=J_{23}^{\pm}=\left((J_{23}^{V\max})^2\pm\frac{\sqrt{A_{1,2}A_{12,3}}}{2J_{12}^2}\right)^{1/2}. \quad (18)$$

They mark the boundaries between classical and nonclassical regions. Important semiclassical limits are obtained if one looks for a geometrical interpretation, to deduce formulas which preserve the original symmetries of the 6*j* symbol. These approaches originate from Ponzano and Regge [12] and were elaborated by others, notably Schulten and Gordon [13]. Starting from the recurrence relationships, we introduce a parameter λ indicating the growth of the angular momentum.

The three-term recursion relationship, Eq. (6), for 6*j* symbols admits an illustration in terms of a geometric interpretation: with some approximations to be detailed below one has finite difference equations (see Ref. [37] Eq. (67) for relationships between recursions and finite difference), Consider the Schulten-Gordon relationships Eqs. (66) and (67) (λ = 1) [13]

$$\left(\frac{F(J_1-1,J_2,J_3)F(J_1-1,L_2,L_3)}{J_1-1}\right)^{1/2}\begin{Bmatrix}j_1-1 & j_2 & j_3\\ l_1 & l_2 & l_3\end{Bmatrix}$$
$$+\left(\frac{F(J_1+1,J_2,J_3)F(J_1+1,L_2,L_3)}{J_1+1}\right)^{1/2}\begin{Bmatrix}j_1+1 & j_2 & j_3\\ l_1 & l_2 & l_3\end{Bmatrix}$$
$$-2\cos\theta_1\left(\frac{F(J_1,J_2,J_3)F(J_1,L_2,L_3)}{J_1}\right)^{1/2}\begin{Bmatrix}j_1 & j_2 & j_3\\ l_1 & l_2 & l_3\end{Bmatrix}\approx 0 \quad (19)$$

and Eq. (69)

$$\cos\theta_1=\frac{\begin{array}{r}2J_1^2L_1^2-J_1^2(-J_1^2+L_2^2+L_3^2)\\ -J_2^2(J_1^2+L_2^2-L_3^2)-J_3^2(J_1^2-L_2^2+L_3^2)\end{array}}{16F(J_1,J_2,J_3)F(J_1,L_2,L_3)}, \quad (20)$$

where $F(a, b, c)$ is "area" of *abc* triangle [Eq. (13)]. Coefficients in Eq. (19) are connected to the geometry of the tetrahedron [12]:

$$\frac{3}{2}VJ_1=F(J_1,J_2,J_3)F(J_1,L_2,L_3)\sin\theta_1. \quad (21)$$

In terms of the finite difference operator $\Delta^2(x)f(x) = f(x+1) - 2f(x) + f(x-1)$:

$$[\Delta^2(J_1)+2-2\cos\theta_1]f(J_1)\simeq 0, \quad (22)$$

where

$$f(J_1)=\left(\frac{V}{\sin\theta_1}\right)^{1/2}\begin{Bmatrix}j_1 & j_2 & j_3\\ l_1 & l_2 & l_3\end{Bmatrix}. \quad (23)$$

We have, explicitly

$$\cos\theta_1=\pm\sqrt{1-\left(\frac{3VJ_1}{2F(J_1,J_2,J_3)F(J_1,L_2,L_3)}\right)^2}. \quad (24)$$

From these formulas, and from that of the volume, we have that

- $V = 0$ implies $\cos\theta_1 = \pm 1$ and establishes the classical domain between $J_{1\min}$ and $J_{1\max}$
- $F(J_1, J_2, J_3) = 0$ or $F(J_1, L_2, L_3) = 0$ establish the definition limits $j_{1\min}$ and $j_{1\max}$

For a Schrödinger type equation

$$\frac{d^2\psi}{dq^2}+p^2\psi=0,\ \hbar^2/2m=1, \quad (25)$$

its discrete analog in a grid having one as a step

$$\psi_{n+1}+(p^2-2)\psi_n+\psi_{n-1}=0 \quad (26)$$

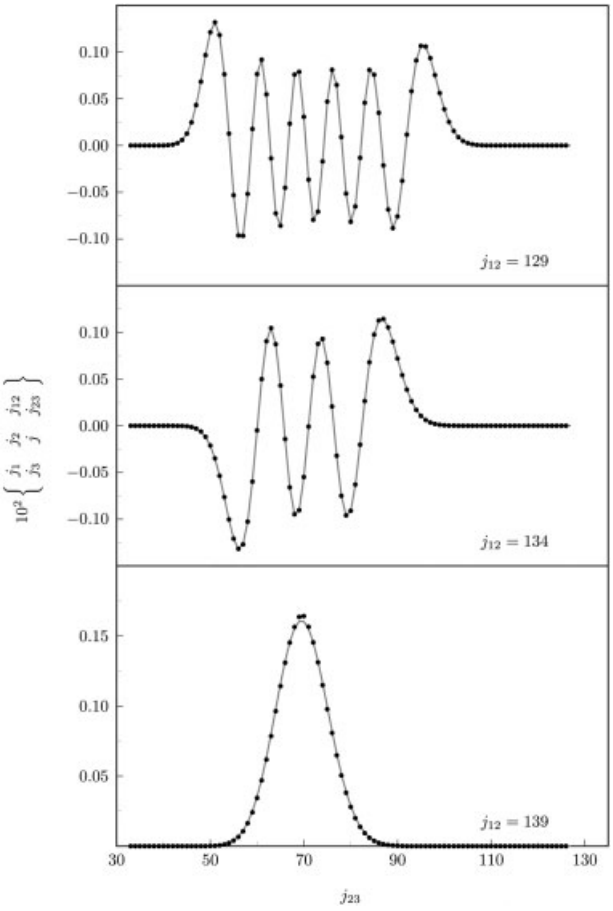

FIGURE 5. 6*j* values as a function of allowed j_{23} for $j_1 = 92$, $j_2 = 47$, $j_3 = 80$, $j = 121$ and the indicated j_{12} values for the three panels. The lines connect the points evaluated by the hypergeometric series of Section 2. The dots are evaluated by the Schulten-Gordon formulas of Section 3. Data available from the authors. Comparison should be made with Figure 3 of Ref. [3].

and so comparing Eq. (26) with Eq. (22) we have

$$f(J_1 + 1) - 2\cos\theta_1 f(J_1) + f(J_1 - 1) = 0 \quad (27)$$

allowing the identification

$$p = \pm (2 - 2\cos\theta_1)^{1/2} \quad (28)$$

Plots corresponding to the three cases of Figure 5 in our Ref. [3], ($\delta = 0$) are given. Clearly, on the closed loop, we can enforce Bohr–Sommerfeld phase space quantization:

$$\oint p dq = (n + 1/2)\pi, \quad (29)$$

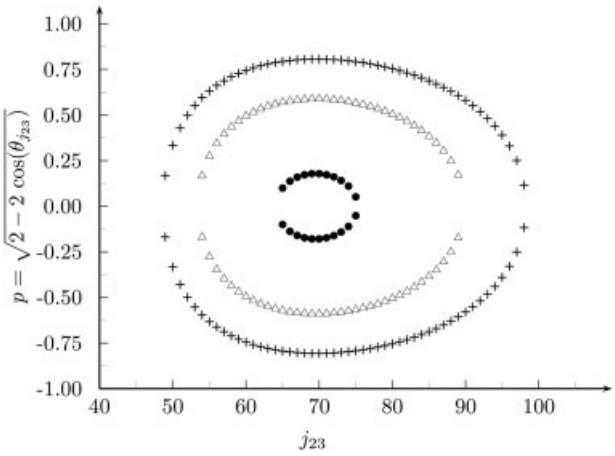

FIGURE 6. Illustration of phase space for semiclassical quantization for $j_1 = 92$, $j_2 = 47$, $j_3 = 80$, $j = 121$, and $j_{12} = 139$ (dots), 134 (triangles), and 129 (plus signs), i.e., the three cases of Figure 5.

where the role of q is played by j_{12}. This is an eigenvalues equations for allowed L_1. The illustration of these formulas is in Figures 6 and 7, with Table I.

3.3. THE 6*j* SYMBOL AND THE OSCILLATOR WAVEFUNCTIONS

The Askey scheme and its counterpart (see Fig. 1) point out at the connection in the angular mo-

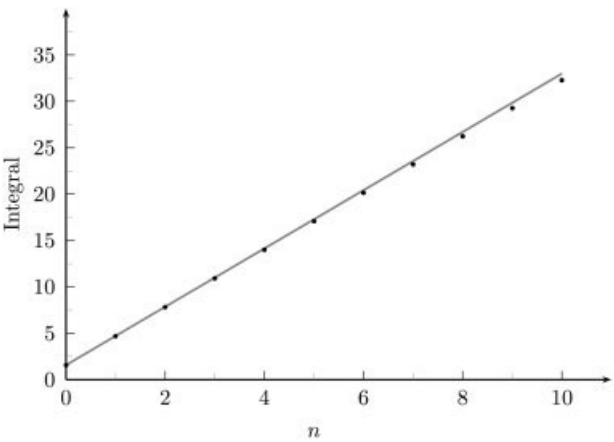

FIGURE 7. Values for the integral of Eq. (29) for different number of nodes *n*. $j_{12} = 139 \rightarrow n = 0$, $j_{12} = 134 \rightarrow n = 5$, $j_{12} = 129 \rightarrow n = 10$. The values of the integrals are connected by the line while the dots are evaluated with p given by Eq. (28).

TABLE I
Values in Eq. (29) and Figure 7.

n	Phase integral	$(n + 1/2)\pi$
0.00	1.569210	1.570796
1.00	4.698102	4.712389
2.00	7.814178	7.853982
3.00	10.917326	10.995574
4.00	14.007433	14.137167
5.00	17.084358	17.278760
6.00	20.147998	20.420352
7.00	23.198198	23.561945
8.00	26.234845	26.703538
9.00	29.257790	29.845130
10.00	32.266890	32.986723

mentum case between the top, the 6*j* symbol, and the bottom, the harmonic oscillator. Indeed the geometrical insight of the Ponzano–Regge theory and its implementation in the Schulten–Gordon asymptotic formulas consistently lead to the expected Airy function behavior astride of the transitions between classical and nonclassical regions of the ranges of elongations of the oscillator. A fully uniform semiclassical treatment involving the mapping of the phase integral over Weber functions appears to be required when the classical region shrinks: this is possibly the origin of inaccuracy of the Schulten–Gordon formulas in the middle of the classical region (see Fig. 5). A simplified direct approach for a particular case is presented in the rest of this section.

The top and bottom of the Askey scheme are the Racah and Hermite polynomials. The geometrical interpretation has been presented in the previous section, here we give an illustration of the case when the phase portraits of Figure 6 can be visualized as ellipses. This "symmetric" case corresponds to $F(J_1, J_2, J_3) = F(J_1, L_2, L_3)$ in previous section, Eq. (24).

In the following we report the connection between harmonic oscillator wavefunctions and 6*j*-coefficients for large angular momentum arguments. In the past Ponzano and Regge [12] (see above) have approximated 6*j*-coefficients with sine and cosine functions as well as Airy functions, and sec II is dedicated to their formulas and extensions by Schulten and Gordon [13], for which we tested as excellent the uniform semi-classical approximation for 6*j*-coefficients. These semi-classical approximations rely on the volume, surface areas, and angles that characterize the tetrahedron that corresponds to each 6*j*-coefficient that is required (See Fig. 3). Here we look at a simple method that connects a large set of special 6*j*-coefficients to harmonic oscillator wavefunctions by using only three parameters that are uniquely given from a simple algebraic analysis of the volumes of some tetrahedra related to the desired set of 6*j*-coefficients.

We consider the approximation of the 6*j*-coefficients:

$$\begin{Bmatrix} j_1 & j_2 & j_{12} \\ j_3 & j & j_{23} \end{Bmatrix}, \tag{30}$$

as a function of j_{12} and j_{23}. These discrete functions are orthonormal with relations:

$$\sum_{j_{12}} (2j_{12}+1)(2j_{23}+1) \begin{Bmatrix} j_1 & j_2 & j_{12} \\ j_3 & j & j_{23} \end{Bmatrix} \begin{Bmatrix} j_1 & j_2 & j_{12} \\ j_3 & j & j'_{23} \end{Bmatrix} = \delta_{j_{23}, j'_{23}},$$

$$\sum_{j_{23}} (2j_{12}+1)(2j_{23}+1) \begin{Bmatrix} j_1 & j_2 & j_{12} \\ j_3 & j & j_{23} \end{Bmatrix} \begin{Bmatrix} j_1 & j_2 & j'_{12} \\ j_3 & j & j_{23} \end{Bmatrix} = \delta_{j_{12}, j'_{12}}. \tag{31}$$

We are interested in comparing the 6*j*-coefficients with one dimensional quantum mechanical harmonic oscillator wavefunctions, which belong to an orthogonal set, so we consider as usual the weighted 6*j*-coefficients:

$$\sqrt{(2j_{12}+1)(2j_{23}+1)} \begin{Bmatrix} j_1 & j_2 & j_{12} \\ j_3 & j & j_{23} \end{Bmatrix}. \tag{32}$$

The "exact" values in the figures are these weighted 6*j*. Duality between j_{12} and j_{23} will reflect in the much less evident duality in the Hermite polynomials between variable and degree [The Hermite polynomials which appear in the orthonormalized harmonics oscillator wavefunctions, see Eq. (35) below]. Some aspect of such a duality have been rediscussed by Askey [38] very recently.

We draw the connection with the harmonic oscillator wave-functions by noting that for given j_1, j_2, j_{12}, j_3, j there will be a value of $j_{23}^{\max}$ that will yield the maximum volume for the corresponding tetrahedron. The volume is given by Eq. (14). The maximum V^2 is obtained by finding the appropriate value of $j_{23}^{\max}$ that gives $\mathrm{d}(V^2)/\mathrm{d}j_{23} = 0$. [See Eq. (15)].

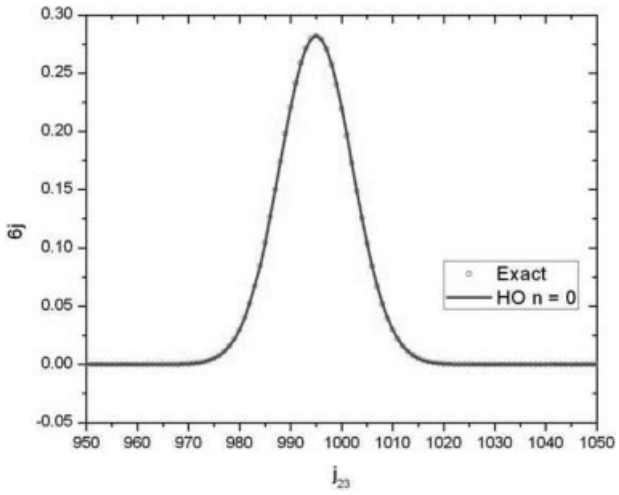

FIGURE 8. Representation of the 6*j* symbols in (33) by the harmonic oscillator wavefuntion [HO, Eq. (34)] for the case $j_1 = 1000$, $j_2 = 1000$, $j_{12} = 200$, $j_3 = 100$, $j = 100$.

Consider the particular 6*j*-symbol:

$$\begin{Bmatrix} j_1 & j_2 & 2j-n \\ j_3 & j & j_{23} \end{Bmatrix}, \tag{33}$$

where $j_2 = j_1$ and $j = j_3$. This symbol has n nodes as j_{23} is varied [3, 6]. Now we can set up the approximation using harmonic oscillator wave functions:

$$\Psi_n(x) = \left(\frac{\alpha}{\pi}\right)^{\frac{1}{4}} \frac{1}{2^{n/2}\sqrt{n!}} H_n(\sqrt{\alpha}x) e^{-\alpha x^2/2} \tag{34}$$

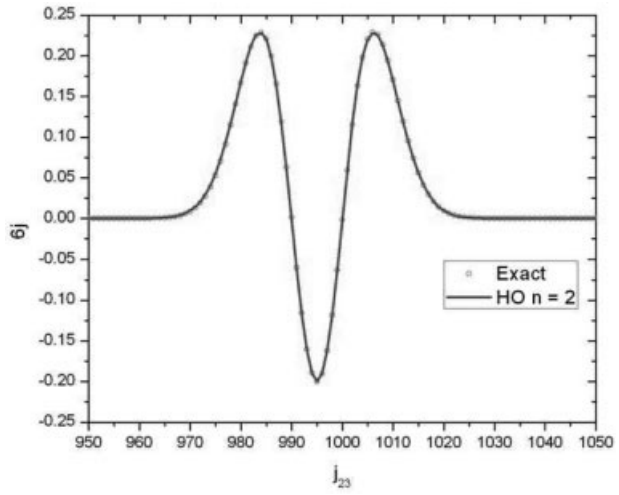

FIGURE 9. As in Figure 8, for $j_1 = 1000$, $j_2 = 1000$, $j_{12} = 198$, $j_3 = 100$, $j = 100$.

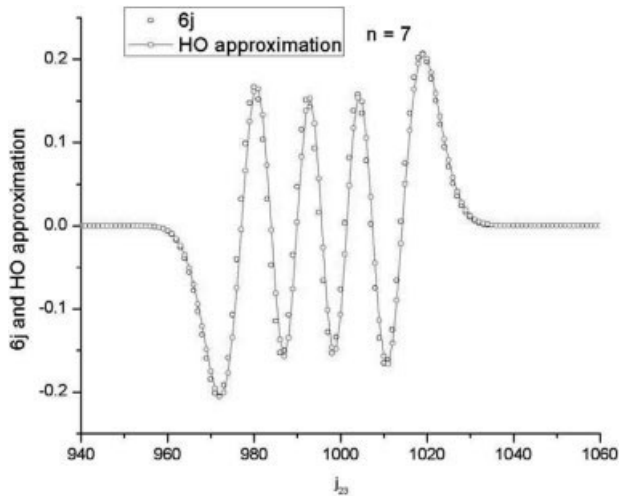

FIGURE 10. As in Figure 8, for $j_1 = 1000$, $j_2 = 1000$, $j_{12} = 193$, $j_3 = 100$, $j = 100$.

where $x = j_{23} - j_{23}^{\max}$, and $\alpha = 4/(j_{23}^{+} - j_{23}^{-})^2$. [See Eq. 18].

Figures 8–10 are based on the 6*j*-symbol:

$$\begin{Bmatrix} 1000 & 1000 & 200-n \\ 100 & 100 & j_{23} \end{Bmatrix} \tag{35}$$

which gives the values for $j_{23}^{\max}$ and α. The figures show $n = 0$, $n = 2$, and $n = 7$.

We see that the harmonic oscillator parameters obtained from the two parameters: $j_{23}^{\max}$ and α pro-

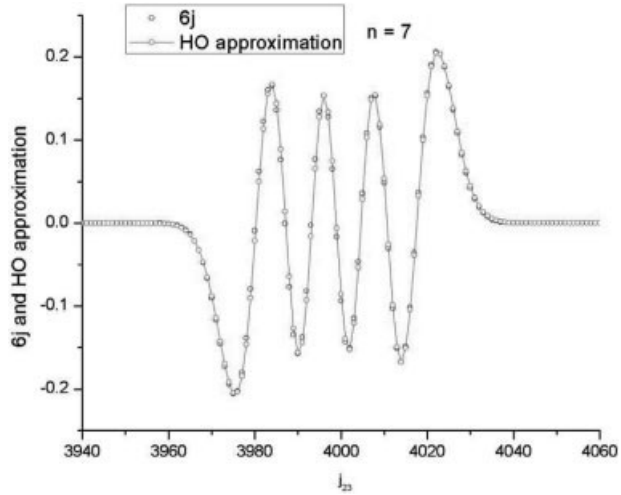

FIGURE 11. As in Figure 8, for $j_1 = 4000$, $j_2 = 4000$, $j_{12} = 200$, $j_3 = 100$, $j = 100$.

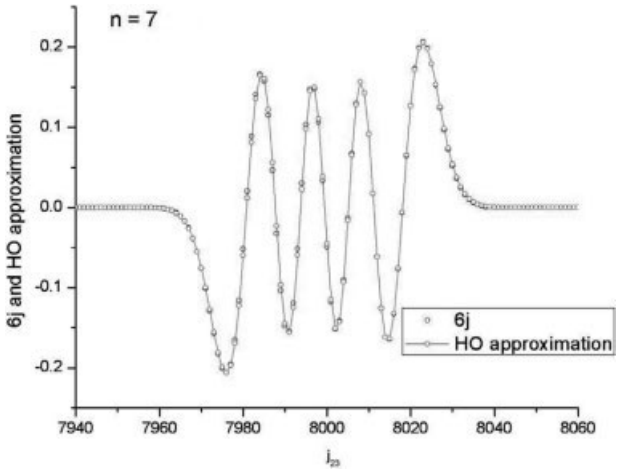

FIGURE 12. As in Figure 8, for $j_1 = 8000$, $j_2 = 8000$, $j_{12} = 200$, $j_3 = 100$, $j = 100$.

vide a remarkable representation of the behavior of specific 6*j*-symbols by harmonic oscillator wavefunctions. The representation for $n = 0$ and $n = 2$ is excellent, but deviations are seen for most j_{23} for $n = 7$. However the agreement gets better for $n = 7$ as j_1 is correspondingly increased, as is shown in Figures 11 and 12.

The present state of the theory shows that the agreement should get better with increasing *j*. Also the theory is expected to accurately represent 6*j* symbols as a linear combination of HO wave functions for smaller values of *j*.

4. Conclusion

In this article we have collected information available on Wigner's 6*j*-symbols (or Racah coefficients), the application of which has been shown to transcend the quantum theory of angular momentum where they originated. The classification schemes and the asymptotic formulas have been elaborated in view of such applications, some of which recently outlined in [1] and [2]. The exact computational machinery, implemented according to Section 2, has already been exploited beyond the examples regarding the 6*j* symbols, of prime interest in this article, but also for the important case of the 9*j* symbols [16], for which asymptotic formulas have been recently derived and tested.

ACKNOWLEDGMENTS

Doctoral fellowships are acknowledged from Brazilian CAPES to ACPB, and from the EU Alban Program to CdSF.

References

1. Aquilanti, V.; Bitencourt, A. C. P.; da Ferreira, C. S.; Marzuoli, A.; Ragni, M. Phys Scr 2008, 78, 058103.
2. Aquilanti, V.; Bitencourt, A. C. P.; da Ferreira, C. S.; Marzuoli, A.; Ragni, M. Theor Chem Acc 2009, DOI:10.1007/S00214-009-0519-y.
3. Aquilanti, V.; Cavalli, S.; Coletti, C. Chem Phys Lett 2001, 344, 587.
4. Nikiforov, A. F.; Suslov, S. K.; Uvarov, V. B. Classical Orthogonal Polynomials of a Discrete Variable; Springer-Verlag: Berlin, 1991.
5. Koekoek, R.; Swarttouw, R. The Askey-scheme of hypergeometric orthogonal polynomials and its q-analogue, Technical report, TU Delft, The Netherlands, 1998. Available at: ftp.twi.tudelft.nl, directory:/pub/publications/tech-reports.
6. Aquilanti, V.; Coletti, C. Chem Phys Lett 2001, 344, 601.
7. Aquilanti, V.; Cavalli, S.; Coletti, C.; Di Domenico, D.; Grossi, G. Int Rev Phys Chem 2001, 20, 673.
8. Aquilanti, V.; Caligiana, A.; Cavalli, S.; Coletti, C. Int J Quantum Chem 2003, 92, 212.
9. De Fazio, D.; Cavalli, S.; Aquilanti, V. Int J Quantum Chem 2003, 93, 91.
10. Aquilanti, V.; Haggard, H. M.; Littlejohn, R.; Yu, L. J Phys A 2007, 40, 5637.
11. Anderson, R. W.; Aquilanti, V. J Chem Phys 2006, 124, 214104.
12. Ponzano, G.; Regge, T. In Spectroscopic and Group Theoretical Methods in Physics; Bloch, F.; Cohen, S. G.; de Shalit, A.; Sambursky, S.; Talmi, I., Eds.; North-Holland: Amsterdam, 1968.
13. Schulten, K.; Gordon, R. G. J Math Phys 1975, 16, 1971.
14. Bailey, D. H.; Hida, Y.; Jeyabalan, K. http://crd.lbl.gov/~dhbailey/mpdist/2006.
15. Varshalovich, D. A.; Moskalev, A. N.; Khersonskii, V. K. Quantum Theory of Angular Momentum; World Scientific: Singapore, 1988.
16. Anderson, R. W.; Aquilanti, V.; da Silva Ferreira, C. J Chem Phys 2008, 129, 161101.
17. Zare, R. N. Angular Momentum; Wiley: New York, 1988.
18. Labarthe, J. J. J Phys A: Math Gen 1975, 8, 1543.
19. Roothaan, C. C. J.; Lai, S. T. Int J Quantum Chem 1997, 63, 57.
20. Schulten, K.; Gordon, R. G. Comp Phys Commun 1976, 11, 269.
21. Schulten, K.; Gordon, R. G. J Math Phys 1975, 16, 1961.
22. Wei, L. Q. Comput Phys Commun 1999, 120, 222.
23. Wei, L. Q.; Dalgarno, A. J Phys A: Math Gen 2004, 37, 3259.
24. Stevenson, P. D. Comput Phys Commun 2002, 147, 853.
25. Deveikis, A.; Kuznecovas, A. Comput Phys Commun 2005, 172, 60.

26. Gaigalas, G.; Scharf, O.; Fritzsche, S. Comput Phys Commun 2005, 166, 141.
27. Fritzsche, S.; Inghoff, T.; Tomaselli, M. Comput Phys Commun 2003, 153, 424.
28. Gaigalas, G.; Fritzsche, S. Comput Phys Commun 2002, 149, 39.
29. Fritzsche, S.; Inghoff, T.; Bastug, T.; Tomaselli, M. Comput Phys Commun 2001, 139, 314.
30. Wang, J. B.; Williams, J. F. Comput Phys Commun 1993, 75, 275.
31. Draeger, T. Comput Phys Commun 2001, 139, 246.
32. Reinsch, M. W.; Morehead, J. J. J Math Phys 1999, 40, 4782.
33. Roberts, J. Geometry and Topology 1999, 3, 21.
34. Aquilanti, V.; Cavalli, S.; De Fazio, D. J Phys Chem 1995, 99, 15694.
35. Aquilanti, V.; Capecchi, G. Theor Chem Acc 2000, 104, 183.
36. Freidel, L.; Louapre, D. Classical Quantum Gravity 2003, 20, 1267.
37. Neville, D. J Math Phys 1971, 12, 2438.
38. Askey, R. J Comp App Math 2005, 178, 37.